Net community production in the South China Sea Basin estimated from *in situ* O$_2$ measurements on an Argo profiling float

Yibin Huang[a,b], Bo Yang[c,*,1], Bingzhang Chen[d], Guoqiang Qiu[a], Haili Wang[a], Bangqin Huang[a,b,**]

[a] *State Key Laboratory of Marine Environmental Science, Xiamen University, Xiamen, China*
[b] *Fujian Provincial Key Laboratory of Coastal Ecology and Environmental Studies, Xiamen University, Xiamen, China*
[c] *School of Oceanography, University of Washington, Seattle, USA*
[d] *Ecosystem Dynamics Research Group, Research and Development Center for Global Change, Japan Agency for Marine-Earth Science and Technology, Yokohama, Japan*

ARTICLE INFO

ABSTRACT

For the first time, the net community production (NCP) was estimated over a complete annual cycle in the basin of the South China Sea (SCS) using *in situ* oxygen measurements from an Argo profiling float and an oxygen mass balance model. The annual NCP from July 2014 to July 2015 was estimated to be 2.7 mol C m^{-2} yr^{-1} (calculated to the deepest winter mixed layer depth of 56 m), with the uncertainties ranging from 0.9 ~ 2.2 mol C m^{-2} yr^{-1}. NCP estimates followed a monsoonal pattern with higher values in the cold season (November to April) when northeast monsoon prevailed and low values in the warm season (June to September) when this area was dominated by the southwest monsoon. Most of the net heterotrophic events occurred in the warm season. The magnitude and seasonal pattern derived from our results agree with previous export production studies based on discrete measurements. Comparison with satellite-derived NCP revealed that the results derived with NPP from Carbon-based Production Model (CbPM) were closer to the Argo measurements than the results derived with NPP from Vertically Generalized Production Model (VGPM) in magnitude; while the VGPM-based approach did a better job in reproducing the seasonal cycle of NCP in this area. This novel approach provides the possibilities to study the carbon cycle in the SCS with a much higher temporal and spatial resolution, as well as more insights for metabolic state in the oligotrophic subtropical gyres.

1. Introduction

The biological transfer and export of organic carbon from the surface ocean into the deep sea, commonly referred to as the marine biological pump, plays an important role in regulating the atmospheric CO$_2$ level (Sigman and Boyle, 2000; Ciais et al., 2013). At steady state, the magnitude of net community production (NCP), defined as the gross primary production minus the community respiration, equals to the amount of biologically-produced organic matter available for export and hence can be regarded as one of the best proxies to quantify carbon export efficiency of marine biological pump (Del Giorgio and Duarte, 2002; Ducklow and Doney, 2012).

Whether the metabolic state in the oligotrophic subtropical gyres is autotrophic or heterotrophic is still under extensive debate (Ducklow and Doney, 2012; Duarte et al., 2013; Williams et al., 2013): shipboard based incubation (*in vitro*) approaches (mostly light-dark bottle incubations) tend to yield heterotrophy whereas most results from

incubation-free (*in situ*) methods suggest autotrophy in these oligotrophic waters. The major cause for this discrepancy probably lies in the biases associated with one or both types of methodologies (*in vitro* and *in situ*). Also, it can be induced by sampling bias (*e.g.* the two different methods measured NCP at different time and/or locations). The controversy over the sign of NCP cannot be easily solved due to the complicated controlling mechanisms on NCP, which is not only affected by the local primary production, but also related to the dynamics of trophic status and dissolved organic carbon distribution (Arístegui and Harrison, 2002; Serret et al., 2015). If there is some mechanism to deliver semi-labile organic matters from coastal areas to the ocean gyre, the persistent heterotrophic state of the oligotrophic ocean gyre suggested by the *in vitro* measurements could be real (Duarte et al., 2013).

Satellite-based algorithms have been widely utilized to determine the global distribution of NCP and/or particulate export production. Westberry et al. (2012) calculated global NCP using empirical relationships between *in vitro* photosynthesis /respiration and Carbon-

---

based Productivity Model (CbPM, Behrenfeld et al., 2005). Using satellite observations of net primary production and particle size distribution, Siegel et al. (2014) developed a food-web model to estimate the global particulate export production. Li and Cassar (2016) presented two statistical algorithms for predicting global NCP based on satellite observations and *in situ* O_2/Ar-NCP measurements. Satellite-based NCP estimates show strong geographic variability with high values in the equator and the subarctic ocean but low NCP in the subtropical gyres. However, this latitudinal trend has been recently challenged by local observations. For example, Emerson (2014) summarized the global observations of annual NCP in the open ocean, ranging from 2 to $4\,\mathrm{mol\,C\,m^{-2}\,yr^{-1}}$ without significant latitudinal tendency. This problem remains unsolved due to the limited *in situ* observational estimates available for validation of satellite remote sensing algorithms.

Recently, continuous *in situ* observations of chemical tracers (*e.g.* oxygen, nitrate) using autonomous profiling floats and gliders provide a new approach for NCP measurements (*e.g.* Nicholson et al., 2008; Riser and Johnson, 2008; Bushinsky and Emerson, 2015; Plant et al., 2016; Yang et al., 2017). The best advantage of this approach is that, besides providing long-term, high temporal-resolution measurements of oxygen, it is incubation free, thereby circumventing most of the problems of the shipboard light-dark bottle measurements. It is also suitable for remote areas that are under-sampled.

We take the advantage of the availability of a floating Argo equipped with ship-board calibrated oxygen sensor already deployed in the basin of the South China Sea (SCS), which is the largest subtropical marginal sea in the world. The SCS is strongly affected by seasonal monsoons, which drive the surface circulation to an anti-cyclonic gyre in the summer and to a cyclonic gyre in the winter (Hu et al., 2000). Southwest monsoon is predominant between June and September, while the northeast monsoon starts in October and dominates the winter until early spring. The transition between these two monsoon periods takes places in May and October. Under the influence of the East Asian Monsoon System, distinctive seasonal variations have been observed in different biogeochemical parameters such as nutrients (Wong et al., 2007; Du et al., 2013), net primary production (Ning et al., 2004; Tan and Shi, 2009), new production (Lee Chen, 2005), and dissolved organic carbon (Wu et al., 2015). Studies based on ^{14}C incubation method in the SCS have shown the net primary production changing from $45\,\mathrm{mmol\,C\,m^{-2}\,d^{-1}}$ in the winter to a lower value of $32\,\mathrm{mmol\,C\,m^{-2}\,d^{-1}}$ in the summer (Ning et al., 2004). A mean primary production value of $29\,\mathrm{mmol\,C\,m^{-2}\,d^{-1}}$ in the SCS was estimated based on remote sensing (SeaWiFS) data (Liu et al., 2002). Annual export production in the SCS have also been estimated by various approaches such as ^{234}Th-based particular organic carbon (POC) exports (Cai et al., 2015; Chen et al., 2008), sediment traps (Chen et al., 1998), numerical models (Liu et al., 2002; Liu and Chai, 2009), ^{15}NO$_3$ uptake incubation experiments (Lee Chen, 2005), and nutrients budgets (Hung et al., 2007), with a range of $0.8–3.1\,\mathrm{mol\,C\,m^{-2}\,yr^{-1}}$. For direct measurements of NCP in this area, however, there is only one field study conducted in the summer using the light-dark bottle method (Wang et al., 2014). The results therein showed that in the summer the autotrophic state dominated the coastal area whereas the net heterotrophic state dominated the SCS basin. The lack of temporal and spatial coverage for NCP studies remains a critical issue for further evaluation of the biological pump efficiency and carbon cycling in the SCS. Here, we strive to obtain high temporal resolution of NCP estimates in the SCS basin based on the continuous O_2 measurements on an Argo profiling float. Our aim is to provide a more comprehensive and unbiased picture of NCP in the SCS basin and, more broadly, to add more insights into the unresolved debate on the autotrophy *versus* heterotrophy in oligotrophic ocean gyres.
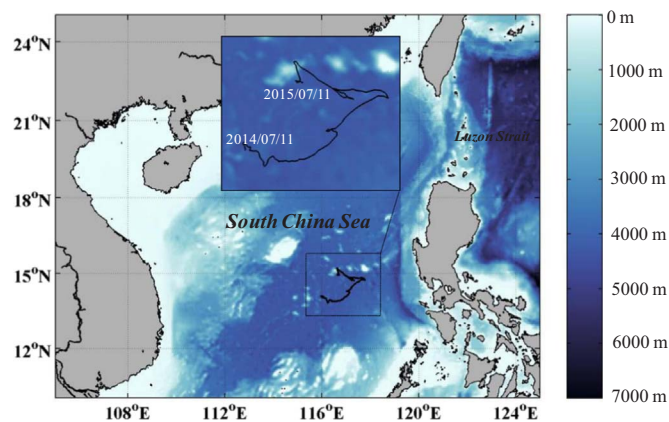

Fig. 1. Study area in the basin of the South China Sea. The black line represents the Argo float trajectory. The sampling period is from July 11th, 2014 to July 11th, 2015.

2. Materials and methods

2.1. Study area

The study area (13.8°N–15.2°N, 115.9–117.8°E) is located in the center of the SCS basin (Fig. 1). This area is characterized as a tropical oligotrophic environment due to the stratification and isolation by circulation gyres (Ning et al., 2004; Wong et al., 2007), with relatively low surface chlorophyll *a* (Chl-*a*) concentrations ranging from 0.02 to $0.24\,\mu g\,\mathrm{L}^{-1}$ (Zhang et al., 2016). In the summer when strong stratification occurs, both concentrations of nitrate and phosphorus in the upper layer are usually below the detection limit ($0.3\,\mu$M for nitrate and $0.01\,\mu$M for phosphorus, Wong et al., 2007). In the winter, the sea surface is cooled by the northeast monsoon and the mixed layer deepens (Wong et al., 2007). As a result, more nutrients can be entrained into the euphotic zone in the winter and lead to greater phytoplankton biomass and primary production (Liu et al., 2002; Lee Chen and Chen, 2006). For comparison, the time period from November to April of the following year is defined as the cold season when northeast monsoon prevails, and the time period from June to September is defined as the warm season when southwest monsoon prevails.

2.2. Argo deployment and oxygen sensor calibration

The Argo profiling float (Sea-Bird Navis BGCi, No. F0348) used in this study was equipped with a SBE 41CP CTD, a SBE 63 optical dissolved oxygen sensor, and a WET Labs ECO-MCOMS fluorometer (Zhang et al., 2016). The profiling cycle was set to be 1–5 days. The vertical resolution was approximately 2 m from surface to 1000 m depth and 50 m below 1000 m depth. 143 profiles were obtained from July 11th, 2014 to July 11th, 2015. The raw O_2 data were calibrated against discrete samples collected from the CTD cast at the time of float deployment ($0 - 150$ m, measured using spectrophotometric Winkler method, Pai et al., 1993). A linear regression yielded the following calibration equation: $[O_2]_{Winkler} = 1.0912\,(\pm\,0.017) \times [O_2]_{Sensor} - 11.658\,(\pm\,3.025)$ ($R^2 = 0.977$, $n = 6$, Fig. S1). The details of calibration are presented in the Supplementary material.

2.3. Upper ocean oxygen mass balance model

The float data (temperature, salinity, $[O_2]$) were binned into 2-week average and then interpolated into a model grid with 1-m depth resolution and one-day time interval. We adopted a simplified two-layer O_2 mass balance model (Yang et al., 2017) to estimate the NCP in the upper ocean (Fig. 2). Layer 1 represents the mixed layer, which was determined using the temperature-based criteria (the depth with 0.2 °C temperature difference from 10 m, De Boyer Montégut et al., 2004).
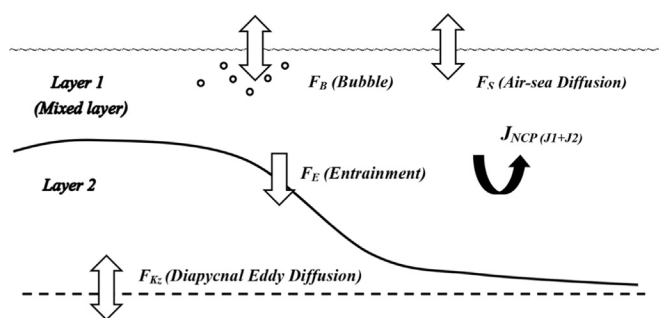
Fig. 2. The schematic of an upper ocean oxygen mass balance model for estimation of net community production. The base of layer 2 was defined as the deepest mixed layer depth of the year (~56 m in this study). Air-sea diffusion flux (F_S) and bubble injection flux (F_B) were calculated using the Liang et al. (2013) gas exchange model. J_{NCP}: net bio-generated oxygen flux.

Table 1
Uncertainties of annual net community production calculated from the upper ocean oxygen mass balance model. k_s, k_p and k_c represent the gas exchange transfer coefficients for calculations of air-sea gas diffusion flux and bubble injection fluxes from the small and large bubbles, and Kz represents the coefficients for diapycnal diffusion calculation (see Supplementary Material for details).

Parameter	Uncertainty (%)	Uncertainty (mol C m^{-2} yr^{-1})
O_2	0.2	± 0.38
	1.0	± 1.7
k_s	10	± 0.24
k_p	50	± 0.15
k_c	50	± 0.10
$k_p + k_c$	50 + 50	± 0.17
K_z	50	± 0.23
All	-	± 0.9 (with O_2 uncertainty of 0.2%)
		± 2.2 (with O_2 uncertainty of 1.0%)

Organic matter exported from the shallower summer mixed layer would be respired in the deeper winter mixed layer and released back to atmosphere as CO_2 (Körtzinger et al., 2008; Palevsky et al., 2016a). Therefore, the deepest winter mixed layer depth (~56 m in this case) was set to be the base of the second layer (Layer 2) for the calculation of the annual net community production (ANCP) in the upper ocean.

The O_2 fluxes in these two layers (d(h[O_2]) / dt, mmol O_2 m^{-2}) are mainly controlled by the fluxes from the following processes: air-sea gas diffusion (F_S, mmol O_2 m^{-2}), bubble injection (F_B, mmol O_2 m^{-2}), entrainment (F_E, mmol O_2 m^{-2}), diapycnal eddy diffusion (F_{Kz}, mmol O_2 m^{-2}), horizontal and vertical advection, and net community production (J_{NCP}, mmol O_2 m^{-2}). Horizontal and vertical advections are much less effective in influencing the gas tracers like oxygen because of the relatively short residence time for O_2 with respect to gas exchange (2–3 weeks) and hence were considered to be negligible in this study (the details are presented in the Supplementary material).

Changes of O_2 in layer 1 (d(h$_1$[O_2]) / dt) are described in Eq. (1), as the sum of fluxes from air-sea gas diffusion (F_S), bubble injection (F_B), entrainment (F_E) and flux from net community production (J_{NCP1}).

$$d(h_1[O_2])/dt = F_S + F_B + F_E + J_{NCP1} \qquad (1)$$

Changes of O_2 in layer 2 (d(h$_2$[O_2]) / dt) are results of entrainment (F_E), diapycnal eddy diffusion (F_{Kz}), and flux from net community production (J_{NCP2}).

$$d(h_2[O_2])/dt = F_{Kz} + F_E + J_{NCP2} \qquad (2)$$

The sum of J_{NCP1} and J_{NCP2} represents the total flux of oxygen from net community production in the upper ocean. In the above equations, O_2 fluxes from sea to air were defined as positive. The details for the calculation of oxygen fluxes in Eq. (1) and Eq. (2) are presented in the Supplementary material.

2.4. Uncertainty analysis

Monte Carlo approach was used to quantify the main sources of uncertainty in ANCP estimates. Randomly-distributed uncertainties were generated for oxygen measurements and each coefficient in the model parameterization (Table 1) and two thousand iterations were run for each variation of those terms. The uncertainties for O_2 measurements can only be precisely estimated when the sensor are frequently calibrated during the deployment. So far, the *in-situ* calibration is only available on Argo floats with air-calibration mechanism (Bushinsky and Emerson, 2015; Bushinsky et al., 2016; Yang et al., 2017) and the uncertainty of O_2 measurements on these floats was estimate to be ± 0.1–0.2%. For floats without air-calibration mechanism, like the one used in this study, it is difficult to precisely estimate the uncertainty for O_2 measurement. Therefore, we used the shipboard oxygen measurement uncertainty (0.2%) as the lower limit, and the Student's t

uncertainty of the calibration equation in Section 2.2 (1% using a 95% confidence interval, see Supplementary material for details) as the upper limit. Following Bushinsky and Emerson (2015) and Yang et al. (2017), the uncertainties of coefficient in air-sea gas diffusion (k_s), coefficients for bubble injection flux from the small bubbles (k_p) and large bubbles (k_c), and diapycnal diffusive coefficient (K_z) were set to be 10%, 50%, 50%, and 50%, respectively.

2.5. Satellite-based NCP estimates

Satellite-based NCP was derived as the net primary production (NPP) multiplied by the ratio of export production to net primary production (e-ratio). Monthly NPP estimates were from the remote sensing data products (http://www.science.oregonstate.edu/ocean.productivity/), using both the Vertically Generalized Production Model (VGPM) (Behrenfeld and Falkowski, 1997), and the Carbon-based Production Model (CbPM) (Behrenfeld et al., 2005). We used the e-ratio (Eq. (3)) from Laws et al. (2011) for this study, which is based on global dataset compiled from field measurements using different methods (chemical tracers, incubation studies, and sediment traps).

$$e - ratio = 0.04756(0.78 - 0.43T/30)\ NPP^{0.37} \qquad (3)$$

3. Results

The evolution of oxygen concentration and supersaturation (ΔO_2 (%) = ([O_2]/[O_2]$_{sat}$ −1)×100) over the course of a year are shown in Fig. 3. The mixed layer depth showed a seasonal cycle with shoaling starting from mid-January and enhanced mixing starting from September (black line in Figs. 3a and 3b). Mixed layer depth determined from the temperature algorithm matched well with the uniform O_2 concentration and supersaturation in the mixed layer (Fig. 3). Low oxygen concentrations were observed in the mixed layer in the summer while high values were found in the winter (Fig. 3a), mainly due to the temperature effect (Fig. S2). O_2 within the mixed layer was supersaturated for the whole year, with higher values (~2.3%) in the summer and lower values (~1.2%) in the winter (Fig. 3b). Significant O_2 maximum layer can be found below the mixed layer from February to August (Fig. 3a).

Wind speed during the cold (Northeast Monsoon) season was generally higher than that during the warm (Southwest Monsoon) season (Fig. 4a). However, in early July of 2014 when typhoon Rammasun was in the SCS, high wind speeds (up to 11 m s^{-1}) were observed along the float track (Fig. 4a). The distribution of surface Chl-*a* generally followed the pattern of wind speed, with over all higher values in the cold season, lower values in the warm season, and a peak value right after the high-wind speed (typhoon) period in early July of 2014 (Fig. 4b).

Daily oxygen fluxes calculated from the upper ocean oxygen mass balance model are presented in Fig. 4b (only four most important fluxes
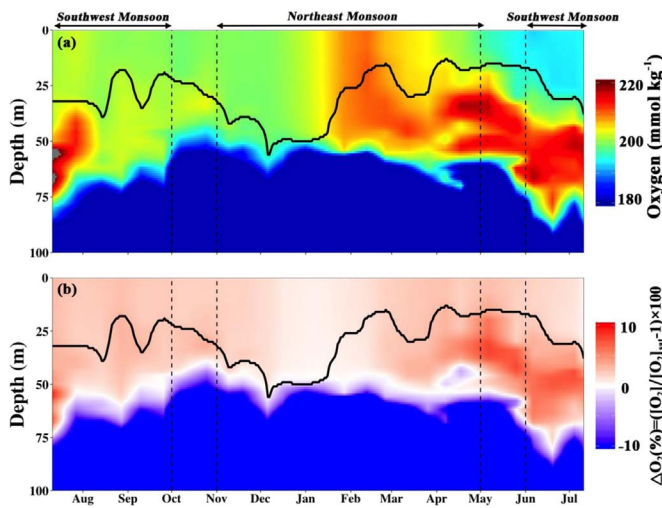
Fig. 3. (a) Oxygen concentration (b) Oxygen supersaturation ΔO_2 (%) = ($[O_2]/[O_2]_{sat}$ –1)×100) as a function of depth (0–100 m) and time from July 2014 to July 2015. The black line represents mixed layer depth.
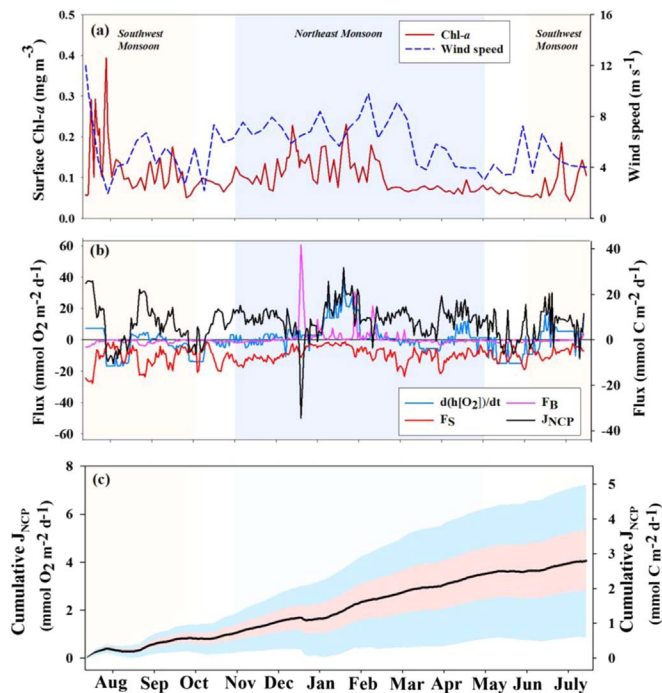

Fig. 4. (a) Weekly surface chlorophyll *a* (Chl-*a*) from Argo float and 10-m wind speed along the profiling float track; (b) Major daily oxygen fluxes in the upper ocean of 56 m, including air-sea diffusion flux (F_S, red), bubble injection flux (F_B, pink), changes of oxygen concentration in the upper ocean (d(h[O_2])/dt, blue) and oxygen flux from net community production the upper (J_{NCP}, black). Fluxes into the ocean are defined as positive. (c) Cumulative net community production (NCP) in the upper ocean from July 2014 to July 2015. Red and blue shadings represent uncertainties of cumulative NCP estimated with the Monte Carlo approach, with oxygen uncertainties of ± 0.2% and ± 1%, respectively. C:O = 1:1.45 was used to covert oxygen flux to carbon production (Hedges et al., 2002). (For interpretation of the references to color in this figure legend, the reader is referred to the web version of this article.)

are shown, a similar figure with all fluxes displayed are presented as Fig. S3a in the Supplementary material). d(h[O_2]) / dt (blue line in Fig. 4b) was the oxygen changes observed by the Argo float. The effect of air-sea gas diffusion (F_S, red line in Fig. 4b) removing O_2 from seawater was significant throughout the year except in the winter period when the O_2 supersaturation decreased (Fig. 3b). Compared with the air-sea gas diffusion, other physical fluxes were much smaller. The

bubble flux (F_B, pink line in Fig. 4b) played minor roles except for the period between December and February of the following year. Diapycnal eddy diffusion (F_{Kz}, see Fig. S3a) became evident from mid-December to March, caused by the relatively strong O_2 concentration gradient across the base of layer 2 (Fig. 3a). The entrainment flux (F_E, see Fig. S3a) was only significant during the period when the rapid changes of mixed layer depth occurred (*e.g.* September and December, Fig. 3). Daily J_{NCP} (black line in Fig. 4b) showed a large variation with relatively high values in January and most negative values in the warm season (*e.g.* May, mid-July to mid-August and the end of September). Monthly cumulative NCP (black line with red squares in Fig. 6) showed a clearer monsoon-forced pattern with higher average values (0.29 mol C m^{-2} monthly^{-1}) in the cold season when the northeast monsoon prevailed (blue shaded area in Fig. 6), approximately 1.6 times of the counterparts (0.17 mol C m^{-2} month^{-1}) in the warm periods under the southwest monsoon (yellow shaded area in Fig. 6). The ANCP was estimated to be 2.7 mol C m^{-2} yr^{-1} (Fig. 4c).

Results of uncertainty analysis are presented in Table 1. The biggest uncertainty of ANCP estimate was from the uncertainty of O_2 measurements. Other significant uncertainties were introduced from the gas diffusion coefficient, and the diapycnal eddy diffusion coefficient. The lower and upper limits of combined uncertainty are presented as red and blue shadings in Fig. 4c, with uncertainties in ANCP of ± 0.9 and ± 2.2 mol C m^{-2} yr^{-1}, respectively.

4. Discussion

4.1. Oxygen fluxes and NCP calculated from the upper ocean oxygen mass balance model

In this upper ocean oxygen mass balance model, the net bio-generated oxygen flux (J_{NCP}) was estimated by subtracting modeled physical oxygen fluxes from the float-measured oxygen changes in the upper ocean, and then J_{NCP} was converted to NCP using an oxygen to carbon ratio of 1.45 (Hedges et al., 2002). The annual cumulative oxygen flux of each term is presented in Fig. 5. Net biological production (J_{NCP}) produced 3.91 mol m^{-2} yr^{-1} oxygen while bubble injection (F_B) and entrainment (F_E) added the other 0.26 mol m^{-2} yr^{-1} oxygen. Meanwhile, the air-sea gas diffusion (Fs) and diapycnal eddy diffusion (F_{Kz}) removed 3.54 and 0.64 mol m^{-2} yr^{-1} oxygen from the upper ocean. Over the course of a year, there was only a small increase (0.01 mol m^{-2} yr^{-1}) in the oxygen budget of the upper ocean.

Since the air-sea O_2 gradient differs by only a few percentages from the atmospheric equilibrium, a small uncertainty in the O_2 measurements could easily cause large uncertainties in NCP. In this study, uncertainty of O_2 measurements caused a significant uncertainty in ANCP (Table 1). Similarly, Yang et al. (2017) showed that an oxygen
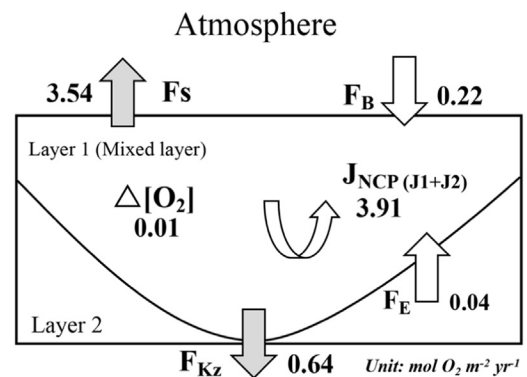

Fig. 5. A schematic of the annual oxygen mass balance in the upper ocean from July 2014 to July 2015. $\Delta[O_2]$: measured oxygen change in the upper ocean, F_S: air-sea diffusion flux, F_B: bubble injection flux, F_{Kz}: diapycnal eddy diffusion flux, F_E: entrainment flux, J_{NCP}, net bio-generated oxygen flux.

concentration offset of 0.2–0.3% led to a difference of 0.4 mol C m^{-2} yr^{-1} in ANCP at the subarctic Ocean Station Papa (OSP). Therefore, accuracy of float oxygen measurement is the key of this oxygen mass balance approach for NCP estimates. An air calibration mechanism has been applied to improve the accuracy of the float oxygen measurements (Bushinsky et al., 2016) and used at both OSP (Bushinsky and Emerson, 2015) and the subtropical Pacific Ocean (Yang et al., 2017). With this air calibration method, ANCP uncertainty from oxygen measurements could be brought down to ~0.2 mol C m^{-2} yr^{-1} (Bushinsky and Emerson, 2015). Due to the hardware limitations, we were not able to perform air calibration for the float used in our study. However, this method provides a better big picture of ANCP in the SCS than traditional methods based on discrete sampling (*e.g.,* sediment traps, incubations), for which the uncertainty is even more difficult to estimate. Moreover, our practice also demonstrates a possible solution to estimate the ANCP distributions with the historical and ongoing oxygen measurements from hundreds of Argo floats without air-calibration mechanism.

The fluxes of air-sea gas exchanges (including air-sea gas diffusion and bubble injection) dominated the physical processes in the upper ocean oxygen mass balance model (Figs. 4b and 5), and thereby the uncertainties from the parameterization of air-sea gas exchange were important for NCP estimates (Table 1). The air-sea gas exchange model of Liang et al. (2013), which incorporates explicit bubble processes, has been proved to be reasonably accurate and adopted by several studies for NCP estimates (Bushinsky and Emerson, 2015; Plant et al., 2016; Yang et al., 2017). In this model, the bubble flux (F_B) consists the flux from small bubbles that totally collapse (F_c), and flux of gas exchange between large bubbles and surrounding water (F_p). Bubble fluxes of this model played an important role in the NCP estimates, particularly in the wintertime with high wind speeds (12–15 m s^{-1}) (Bushinsky and Emerson, 2015; Plant et al., 2016). Furthermore, Yang et al. (2017) optimized the bubble mass transfer coefficients (k_c and k_p) for F_c and F_p, based on the nitrogen measurements at OSP, and suggested a correction factor β of 0.53 for both k_c and k_p. In our case, the bubble flux was relatively small since the average wind speed was much lower (~6 m s^{-1}) and more constant in the SCS (Fig. 4a). Additionally, influx from atmosphere into the ocean caused by the wind-driven small bubbles (F_c) was balanced by the diffusive efflux from the large bubbles (F_p) in the SCS (Fig. S3b), due to the fact that oxygen in the mixed layer was supersaturated for most of the year (Fig. 3b). Therefore, applying the corrected k_c and k_p of Yang et al. (2017) to our model in the SCS only resulted in an insignificant change (~0.1 mol C m^{-2} yr^{-1}) in ANCP.

4.2. Temporal variability of NCP

The monthly cumulative NCP measured from Argo float showed a typical monsoon-forced seasonal distribution in the SCS basin (black line with red squares in Fig. 6), with higher NCP in the cold season when northeast monsoon dominated (blue shaded area) and low NCP values in the warm season when southeast monsoon dominated (yellow shaded area). Such pattern is in good agreement with previous studies of export production using numerical models (Liu et al., 2002; Liu and Chai, 2009) and *in situ* observations (Chen et al., 1998; Lee Chen, 2005) in the open SCS. This pattern is also very similar to the seasonal surface Chl-*a* distribution pattern observed by the chlorophyll fluorescence on this Argo (Fig. 4a). The weekly mean surface Chl-*a* concentration showed a positive correlation with weekly mean wind speed ($r = 0.45$, $p < 0.01$, n = 52). Correspondingly, we also found a similar positive correlation between weekly mean NCP and weekly mean surface Chl-*a* concentration ($r = 0.54$, $p < 0.01$, n = 52). The correlation between NCP and Chl-*a*, and the correlation between Chl-*a* and wind speed suggest that the elevated NCP in the cold season is most likely triggered by weakened stratification and the increased primary production when the enhanced wind-driven vertical mixing brought more nutrients into
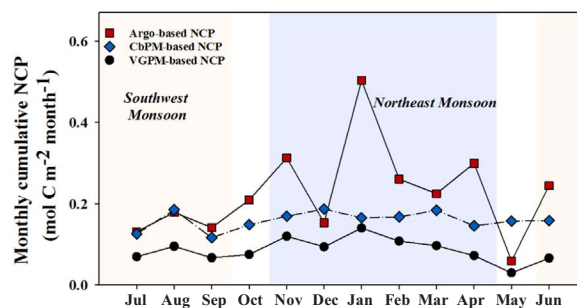

Fig. 6. Comparison of monthly cumulative net community production (NCP) from float oxygen measurements and NCP derived from satellite-based NPP products (CbPM, Carbon-based Production Model and VGPM, Vertically Generalized Production Model). (For interpretation of the references to color in this figure legend, the reader is referred to the web version of this article.)

the euphotic zone from below (Lee Chen and Chen, 2006). Additionally, the shift of plankton community structure can also be an important factor that caused the seasonal variations of NCP (Henson et al., 2012; Cassar et al., 2015). Significant changes of phytoplankton community structure from the smaller pico-phytoplankton (mainly *Prochlorococcus*) in the warm season to the bigger nano-phytoplankton in the cold season have been observed in the SCS basin (Lee Chen, 2005; Chen et al., 2011). They have found that the nano-phytoplankton, including chain-forming diatoms, haptophytes, and prasinophytes, were more abundant in the cold season than in the warm season. All these nano-phytoplankton, compared to pico-phytoplankton, can sink faster due to their larger density, size, and production of "ballast" minerals (Armstrong et al., 2009), which leads to higher carbon export production. Furthermore, the increased portion of bigger, faster-sinking phytoplankton in the cold season can also increase export production by reducing the opportunity for organic carbon to be recycled within the euphotic zone. This hypothesis has been supported by the studies from Cai et al. (2015) in the SCS basin, in which a positive correlation between POC export and the fraction of haptophytes and prasinophytes was reported.

Lower monthly cumulative NCP (yellow shaped area in Fig. 6) and most of short-term negative daily J_{NCP} values (Fig. 4b) were observed in the warm season. The occurrences of short-term negative NCP imply that community respiration exceeds the primary production, consistent with previously reported summer heterotrophic state in the basin of SCS from the result of light-dark bottle experiments (Wang et al., 2014). Lee Chen and Chen (2006) found that the primary production could dramatically decrease due to nutrient limitation around the same time of year when we observed low NCP. Similarly, in our study, the shallow mixed layer in the warm period (black line in Fig. 3) also suggests limited nutrient supply in the euphotic zone due to the stratification when vertical mixing was weak under low wind speed, which could limit primary production, and lead to the decrease in NCP. Another factor for metabolic state shift may be attributed to the increased organic carbon consumption. In the warm season under the nutrient stress, the phytoplankton would release more labile dissolved organic carbon, which could stimulate the bacterial metabolism (Matsumoto et al., 2016). As pointed out by Hoppe et al. (2002), bacterial activity is responsible for the majority of carbon consumption in the oligotrophic areas. The proportion of bacterial respiration to the primary production may be higher under the low primary production in this period, resulting in lower NCP.

4.3. Comparison with previous ANCP estimations in the South China Sea

Our estimated ANCP of 2.7 mol C m^{-2} yr^{-1} is in close agreement with previously estimated new production or export production (Table 2). If assuming a steady state on the annual scale, theoretically NCP should be equivalent to export production and new production, although in practice we still expect nontrivial differences due to the

Table 2
Annual net community production (ANCP) estimated in the South China Sea Basin.

Method	ANCP (mol C m^{-2} yr^{-1})	Description	Reference
Nitrate uptake, Incubation experiment	3.08	Euphotic layer (70–110 m), new production	Lee Chen (2005)
Nutrient budget	2.5	100 m, total organic carbon export	Hung et al. (2007)
^{234}Th equilibrium	2.1	100 m, POC export	Chen et al. (2008)
^{234}Th equilibrium	2.29	100 m, POC export	Cai et al. (2015)
Numerical Model	1.02	125 m, POC flux	Liu et al. (2002)
Numerical Model	1.24	125 m, POC flux, 1990–2004	Liu and Chai (2009)
Sediment trap	0.85–1.07	100 m, POC flux	Chen et al. (1998)
O$_2$ mass balance	2.7	56 m, total organic carbon export	This study

POC: particle organic carbon.

methodology themselves (*e.g.* dissolved organic carbon (DOC) production was left out when using methods based on particle export), the different sampling regimes, and violation of the steady state assumption. Our estimate of ANCP is between the estimates of new production based on ^{15}N and the estimates of export production calculated from ^{234}Th measurements, but substantially higher than model estimates and one sediment trap study 20 years ago (Table 2). Given the substantial uncertainties associated with sampling and methodology, the consistent results among different studies are encouraging, implying the validity of the estimated ANCP and the new approach itself. The much lower estimate from the ocean models suggest substantial deficiency of current plankton models, which typically oversimplify biological diversity and processes. The estimate from Chen et al. (1998) was based on the back-calculation of the POC flux at 1000 m using the normalized depth-dependent function (Martin curve, Martin et al., 1987), which itself has substantial uncertainty. In addition, the POC-based export production measurements ignore the export associated with zooplankton vertical migration (Steinberg et al., 2000), and only account for particulate carbon and do not represent the DOC. It has been reported that the contribution of DOC to global carbon export in the open ocean could be ~20% (Hansell and Carlson, 1998), which can be even higher (50%) in some extreme cases when strong mixing occurred (Carlson et al., 1994).

4.4. Comparison with satellite-derived NCP

A comparison of monthly cumulative NCP values obtained using Argo oxygen observations (black line with red squares) and satellite-based export production estimates (black line with blue diamonds for CbPM-NPP based estimates and black lined with black dots for VGPM-NPP based estimates) is presented in Fig. 6. Our results showed that NCP predicted from CbPM-NPP came closer to our oxygen mass balance estimates, whereas the NCP derived from VGPM-NPP was significantly lower. In the subtropical North Pacific (Hawaii Ocean Time-series, HOT), Palevsky et al. (2016b) also found a similar pattern with the CbPM-based results better reproducing the magnitude of geochemically determined NCP than NCP from VGPM-based approach. For NPP estimates, comparison between field measurements and VGPM estimates in the SCS also showed a similar result, with VGPM estimates significantly lower than field measurements (Tan and Shi, 2009). On the other hand, NCP derived from the VGPM NPP algorithm did a better job in reproducing the seasonality shown by this study and former studies based on discrete measurements (Fig. 6), indicated by stronger correlation in NCP seasonality between VGPM-NPP derived NCP and measured NCP (r = 0.66, p < 0.01 for VGPM-NPP based NCP; r = 0.21, p = 0.94 for CbPM-based NCP; n = 12). Overall, we found that no single NCP estimates derived from satellite NPP models can reproduce both seasonal pattern and magnitude of NCP determined from the *in situ* measurements. This conclusion is similar to those comparisons made by Palevsky et al. (2016b) for the subtropical/subarctic boundary of Pacific Ocean and Yang et al. (2017) for the subtropical Pacific. Thus, more cautions are required when using satellite algorithms for regional predictions of NCP.

4.5. Implication

The SCS is well known as a highly dynamic system with processes such as upwelling, eddy and typhoon, which have great impacts on the biochemical cycle in the SCS (Ning et al., 2004; Zhai et al., 2013; Wang et al., 2016). With higher temporal resolution oxygen data from profiling floats, we were able to capture some abrupt changes in daily NCP (Fig. 4b) during the short-term processes that would be difficult to obtain with traditional approaches based on discrete sampling due to the lack of both temporal and spatial coverages. For example, a large peak of bio-generated oxygen flux (J$_{NCP}$) was observed in July 2014 (Fig. 4b), when the typhoon (tropical cyclone) Rammasun was in the SCS. Although the typhoon's path was about 200 km from our Argo float, the increased wind speed (~10 m s^{-1}) could still be observed on the float path, which was significantly higher than the average wind speed of ~5 m s^{-1} in the warm season (Fig. 4a). The NCP was usually low in the summer due to the stratification, however, it is likely that the typhoon-induced vertical mixing brought more nutrients to fuel biological production in the euphotic zone and led to the elevated NCP, which was also consistent with the rapidly increased Chl-*a* during the same period (Fig. 4a). On the other hand, the spatial resolution of future carbon cycle studies in the SCS can also be enhanced by deploying more autonomous platforms (*e.g.* profiling floats, gliders) with the capability of chemical tracer measurements.

The observed NCP variations also provide us some implications for the debate in metabolic states of the oligotrophic subtropical gyres. Based on the observed heterotrophic and autotrophic events from our high-resolution data, our results imply that the opposite results of metabolic state in the oligotrophic gyres from various studies (*e.g.* Duarte et al., 2013; Williams et al., 2013) might be in part attributed to sampling biases and inappropriate extrapolation. Field studies based on discrete measurements can only capture a "snapshot", and extrapolation from a "snapshot" may lead to a biased conclusion. For example, despite the short-term negative NCP observed in early August (Fig. 4b), the monthly cumulative NCP of August 2014 was still positive and the metabolic state was autotrophic (Fig. 6). On the other hand, if a discrete measurement was taken during the period when NCP was negative (*e.g.* Wang et al., 2014), extrapolating this result to the whole month of August would lead to a wrong conclusion that the metabolic state was heterotrophic in August 2014.

5. Conclusions

For the first time, high temporal resolution NCP estimates were obtained in the SCS basin with oxygen measurements on a profiling float and an upper ocean oxygen mass balance model. The positive ANCP implies a net autotrophy of this oligotrophic system over a complete seasonal cycle. The observed NCP seasonality is consistent with former studies in the SCS based on discrete measurements, with higher NCP in the winter when northeast monsoon prevailed. The large variations in NCP and fast shifting of metabolic states observed in this subtropical oligotrophic environment also suggest that extra caution

should be taken when extrapolating the results from discrete measurements to a larger temporal scale. Comparison with satellite-based export production estimates indicates that no a single satellite algorithm can both reproduce seasonality and magnitude of NCP in the SCS basin. Continuous chemical tracer measurements like Argo oxygen measurements presented here will be necessary for the studies of the highly dynamic carbon system in the SCS.

Acknowledgments

Authors contributions

Bangqin Huang, Haili Wang and Guoqiang Qiu designed and performed the experiment; Yibin Huang and Bo Yang analyzed the data and wrote the paper; Binzhang Chen, Guoqiang Qiu and Bangqin Huang revised the manuscript.

Appendix A. Supporting information

Supplementary data associated with this article can be found in the online version at http://dx.doi.org/10.1016/j.dsr.2017.11.002.

References

Arístegui, J., Harrison, W.G., 2002. Decoupling of primary production and community respiration in the ocean: implications for regional carbon studies. Aquat. Microb. Ecol. 29 (2), 199–209. http://dx.doi.org/10.3354/ame029199.

Armstrong, R.A., Peterson, M.L., Lee, C., Wakeham, S.G., 2009. Settling velocity spectra and the ballast ratio hypothesis. Deep Sea Res. Part II: Top. Stud. Oceanogr. 56 (18), 1470–1478. http://dx.doi.org/10.1016/j.dsr2.2008.11.032.

Behrenfeld, M.J., Boss, E., Siegel, D.A., Shea, D.M., 2005. Carbon-based ocean productivity and phytoplankton physiology from space. Glob. Biogeochem. Cycles 19 (1), 1–14. http://dx.doi.org/10.1029/2004GB002299.

Behrenfeld, M.J., Falkowski, P.G., 1997. Photosynthetic rates derived from satellite-based chlorophyll concentration. Limnol. Oceanogr. 42 (1), 1–20. http://dx.doi.org/10.4319/lo.1997.42.1.0001.

Bushinsky, S.M., Emerson, S., 2015. Marine biological production from *in situ* oxygen measurements on a profiling float in the subarctic Pacific Ocean. Glob. Biogeochem. Cycles 29 (12), 2050–2060. http://dx.doi.org/10.1002/2015gb005251.

Bushinsky, S.M., Emerson, S.R., Riser, S.C., Swift, D.D., 2016. Accurate oxygen measurements on modified Argo floats using *in situ* air calibrations. Limnol. Oceanogr.-Methods 14 (8), 491–505. http://dx.doi.org/10.1002/lom3.10107.

Cai, P.H., Zhao, D.C., Wang, L., Huang, B.Q., Dai, M.H., 2015. Role of particle stock and phytoplankton community structure in regulating particulate organic carbon export in a large marginal sea. J. Geophys. Res.-Oceans 120 (3), 2063–2095. http://dx.doi.org/10.1002/2014jc010432.

Carlson, C.A., Ducklow, H.W., Michaels, A.F., 1994. Annual flux of dissolved organic carbon from the euphotic zone in the northwestern Sargasso Sea. Nature 371 (371), 405–408. http://dx.doi.org/10.1038/371405a0.

Cassar, N., Wright, S.W., Thomson, P.G., Trull, T.W., Westwood, K.J., Salas, M., Davidson, A., Pearce, I., Davies, D.M., Matear, R.J., 2015. The relation of mixed-layer net

community production to phytoplankton community composition in the Southern Ocean. Glob. Biogeochem. Cycles 29 (4), 446–462. http://dx.doi.org/10.1002/2014GB004936.

Chen, B.Z., Wang, L., Song, S.Q., Huang, B.Q., Sun, J., Liu, H.B., 2011. Comparisons of picophytoplankton abundance, size, and fluorescence between summer and winter in northern South China Sea. Cont. Shelf Res. 31 (14), 1527–1540. http://dx.doi.org/10.1016/j.csr.2011.06.018.

Chen, J., Zheng, L., Wiesner, M., Chen, R., Zheng, Y., Wong, H., 1998. Estimations of primary production and export production in the South China Sea based on sediment trap experiments. Chin. Sci. Bull. 43 (7), 583–586. http://dx.doi.org/10.1007/BF02883645.

Chen, W., Cai, P., Dai, M., Wei, J., 2008. ^{234}Th/^{238}U disequilibrium and particulate organic carbon export in the northern South China Sea. J. Oceanogr. 64 (3), 417–428. http://dx.doi.org/10.1007/s10872-008-0035-z.

Ciais, P., Sabine, C., Bala, G., Bopp, L., Brovkin, V., Canadell, J., Chhabra, A., DeFries, R., Galloway, J., Heimann, M., 2013. Carbon and other biogeochemical cycles. In: Stocker, T.F. (Ed.), Climate Change 2013: The Physical Science Basis—Contribution of Working Group I to the Fifth Assessment Report of the Intergovernmental Panel on Climate Change. Cambridge University Press, Cambridge, U.K., New York, pp. 465–570.

De Boyer Montégut, C., Madec, G., Fischer, A.S., Lazar, A., Iudicone, D., 2004. Mixed layer depth over the global ocean: an examination of profile data and a profile-based climatology. J. Geophys. Res.-Oceans 109, C12003. http://dx.doi.org/10.1029/2004JC002378.

Del Giorgio, P.A., Duarte, C.M., 2002. Respiration in the open ocean. Nature 420 (6914), 379–384. http://dx.doi.org/10.1038/nature01165.

Du, C., Liu, Z., Dai, M., Kao, S.-J., Cao, Z., Zhang, Y., Huang, T., Wang, L., Li, Y., 2013. Impact of the Kuroshio intrusion on the nutrient inventory in the upper northern South China Sea: insights from an isopycnal mixing model. Biogeosciences 10 (10), 6419. http://dx.doi.org/10.5194/bg-10-6419-2013.

Duarte, C.M., Regaudie-de-Gioux, A., Arrieta, J.M., Delgado-Huertas, A., Agusti, S., 2013. The oligotrophic ocean is heterotrophic. Annu. Rev. Mar. Sci. 5 5 (4), 551–569. http://dx.doi.org/10.1146/annurev-marine-121211-172337.

Ducklow, H.W., Doney, S.C., 2012. What is the metabolic state of the oligotrophic ocean? A debate. Annu. Rev. Mar. Sci. 5 (1), 525–533. http://dx.doi.org/10.1146/annurev-marine-121211-172331.

Emerson, S., 2014. Annual net community production and the biological carbon flux in the ocean. Glob. Biogeochem. Cycles 28 (1), 14–28. http://dx.doi.org/10.1002/2013gb004680.

Hansell, D.A., Carlson, C.A., 1998. Net community production of dissolved organic carbon. Glob. Biogeochem. Cycles 12 (3), 443–453. http://dx.doi.org/10.1029/98GB01928.

Hedges, J.I., Baldock, J.A., Gélinas, Y., Lee, C., Peterson, M.L., Wakeham, S.G., 2002. The biochemical and elemental compositions of marine plankton: a NMR perspective. Mar. Chem. 78 (1), 47–63. http://dx.doi.org/10.1016/S0304-4203(02)00009-9.

Henson, S., Lampitt, R., Johns, D., 2012. Variability in phytoplankton community structure in response to the North Atlantic Oscillation and implications for organic carbon flux. Limnol. Oceanogr. 57 (6), 1591–1601. http://dx.doi.org/10.4319/lo.2012.57.6.1591.

Hoppe, H.G., Gocke, K., Koppe, R., Begler, C., 2002. Bacterial growth and primary production along a north-south transect of the Atlantic Ocean. Nature 416 (6877), 168–171. http://dx.doi.org/10.1038/416168a.

Hu, J., Kawamura, H., Hong, H., Qi, Y., 2000. A review on the currents in the South China Sea: seasonal circulation, South China Sea warm current and Kuroshio intrusion. J. Oceanogr. 56 (6), 607–624. http://dx.doi.org/10.1023/A:1011117531252.

Hung, J.J., Wang, S.M., Chen, Y.L., 2007. Biogeochemical controls on distributions and fluxes of dissolved and particulate organic carbon in the Northern South China Sea. Deep Sea Res. Part II: Top. Stud. Oceanogr. 54 (14–15), 1486–1503. http://dx.doi.org/10.1016/j.dsr2.2007.05.006.

Körtzinger, A., Send, U., Wallace, D.W.R., Karstensen, J., DeGrandpre, M., 2008. The seasonal pCO$_2$ cycle at 49˚N/16.5˚W in the northeastern Atlantic Ocean and what it tells us about biological productivity. J. Geophys. Res.-Oceans 113 (C4). http://dx.doi.org/10.1029/2007JC004347.

Laws, E.A., D'Sa, E., Naik, P., 2011. Simple equations to estimate ratios of new or export production to total production from satellite-derived estimates of sea surface temperature and primary production. Limnol. Oceanogr.-Methods 9 (12), 593–601. http://dx.doi.org/10.4319/lom.2011.9.593.

Lee Chen, Y.-l., 2005. Spatial and seasonal variations of nitrate-based new production and primary production in the South China Sea. Deep Sea Res. Part I: Oceanogr. Res. Pap. 52 (2), 319–340. http://dx.doi.org/10.1016/j.dsr.2004.11.001.

Lee Chen, Y.-l., Chen, H.-Y., 2006. Seasonal dynamics of primary and new production in the northern South China Sea: the significance of river discharge and nutrient advection. Deep Sea Res. Part I: Oceanogr. Res. Pap. 53 (6), 971–986. http://dx.doi.org/10.1016/j.dsr.2006.02.005.

Liang, J.-H., Deutsch, C., McWilliams, J.C., Baschek, B., Sullivan, P.P., Chiba, D., 2013. Parameterizing bubble-mediated air-sea gas exchange and its effect on ocean ventilation. Glob. Biogeochem. Cycles 27 (3), 894–905. http://dx.doi.org/10.1002/gbc.20080.

Li, Z., Cassar, N., 2016. Satellite estimates of net community production based on O$_2$/Ar observations and comparison to other estimates. Glob. Biogeochem. Cycles 30 (5), 735–752. http://dx.doi.org/10.1002/2015GB005314.

Liu, G., Chai, F., 2009. Seasonal and interannual variability of primary and export production in the South China Sea: a three-dimensional physical-biogeochemical model study. Ices J. Mar. Sci. 66 (2), 420–431. http://dx.doi.org/10.1093/icesjms/fsn219.

Liu, K.-K., Chao, S.-Y., Shaw, P.-T., Gong, G.-C., Chen, C.-C., Tang, T., 2002. Monsoon-forced chlorophyll distribution and primary production in the South China Sea:

observations and a numerical study. Deep Sea Res. Part I: Oceanogr. Res. Pap. 49 (8), 1387–1412. http://dx.doi.org/10.1016/s0967-0637(02)00035-3.

Martin, J.H., Knauer, G.A., Karl, D.M., Broenkow, W.W., 1987. VERTEX: carbon cycling in the northeast Pacific. Deep Sea Res. Part I: Oceanogr. Res. 34 (2), 267–285. http://dx.doi.org/10.1016/0198-0149(87)90086-0.

Matsumoto, K., Abe, O., Fujiki, T., Sukigara, C., Mino, Y., 2016. Primary productivity at the time-series stations in the northwestern Pacific Ocean: is the subtropical station unproductive? J. Oceanogr. 72 (3), 359–371. http://dx.doi.org/10.1007/s10872-016-0354-4.

Nicholson, D., Emerson, S., Eriksen, C.C., 2008. Net community production in the deep euphotic zone of the subtropical North Pacific gyre from glider surveys. Limnol. Oceanogr. 53 (5), 2226–2236. http://dx.doi.org/10.4319/lo.2008.53.5_part_2.2226.

Ning, X., Chai, F., Xue, H., Cai, Y., Liu, C., Shi, J., 2004. Physical-biological oceanographic coupling influencing phytoplankton and primary production in the South China Sea. J. Geophys. Res.-Oceans 109 (C10). http://dx.doi.org/10.1029/2004JC002365.

Palevsky, H.I., Quay, P.D., Lockwood, D.E., Nicholson, D.P., 2016a. The annual cycle of gross primary production, net community production, and export efficiency across the North Pacific Ocean. Glob. Biogeochem. Cycles 30 (2), 361–380. http://dx.doi.org/10.1002/2015gb005318.

Palevsky, H.I., Quay, P.D., Nicholson, D.P., 2016b. Discrepant estimates of primary and export production from satellite algorithms, a biogeochemical model, and geochemical tracer measurements in the North Pacific Ocean. Geophys. Res. Lett. 43 (16), 8645–8653. http://dx.doi.org/10.1002/2016GL070226.

Pai, S.-C., Gong, G.-C., Liu, K.-K., 1993. Determination of dissolved oxygen in seawater by direct spectrophotometry of total iodine. Mar. Chem. 41 (4), 343–351. http://dx.doi.org/10.1016/0304-4203(93)90266-Q.

Plant, J.N., Johnson, K.S., Sakamoto, C.M., Jannasch, H.W., Coletti, L.J., Riser, S.C., Swift, D.D., 2016. Net community production at Ocean Station Papa observed with nitrate and oxygen sensors on profiling floats. Glob. Biogeochem. Cycles 30 (6), 859–879. http://dx.doi.org/10.1002/2015gb005349.

Riser, S.C., Johnson, K.S., 2008. Net production of oxygen in the subtropical ocean. Nature 451 (7176), 323–325. http://dx.doi.org/10.1038/nature06441.

Serret, P., Robinson, C., Aranguren-Gassis, M., Garcia-Martin, E.E., Gist, N., Kitidis, V., Lozano, J., Stephens, J., Harris, C., Thomas, R., 2015. Both respiration and photosynthesis determine the scaling of plankton metabolism in the oligotrophic ocean. Nat. Commun. 6, 6961 (doi:1038/ncomms7961).

Siegel, D.A., Buesseler, K.O., Doney, S.C., Sailley, S.F., Behrenfeld, M.J., Boyd, P.W., 2014. Global assessment of ocean carbon export by combining satellite observations and food-web models. Glob. Biogeochem. Cycles 28 (3), 181–196. http://dx.doi.org/10.1002/2013GB004743.

Sigman, D.M., Boyle, E.A., 2000. Glacial/interglacial variations in atmospheric carbon dioxide. Nature 407 (6806), 859–869. http://dx.doi.org/10.1038/35038000.

Steinberg, D.K., Carlson, C.A., Bates, N.R., Goldthwait, S.A., Madin, L.P., Michaels, A.F., 2000. Zooplankton vertical migration and the active transport of dissolved organic and inorganic carbon in the Sargasso Sea. Deep Sea Res. Part I: Oceanogr. Res. Pap. 47 (1), 137–158. http://dx.doi.org/10.1016/S0967-0637(99)00052-7.

Tan, S.C., Shi, G.Y., 2009. Spatiotemporal variability of satellite-derived primary production in the South China Sea, 1998–2006. J. Geophys. Res.-Biogeosci. 114 (G3). http://dx.doi.org/10.1029/2008JG000854.

Wang, L., Huang, B., Chiang, K.P., Liu, X., Chen, B., Xie, Y., Xu, Y., Hu, J., Dai, M., 2016. Physical-biological coupling in the western South China Sea: the response of phytoplankton community to a mesoscale cyclonic eddy. PLoS One 11 (4), e0153735. http://dx.doi.org/10.1371/journal.pone.0153735.

Wang, N., Lin, W., Chen, B., Huang, B., 2014. Metabolic states of the Taiwan Strait and the northern South China Sea in summer 2012 (In Chinese with English abstract). J. Trop. Oceanogr. 33 (4), 61–68.

Westberry, T.K., Williams, P.J.L.B., Behrenfeld, M.J., 2012. Global net community production and the putative net heterotrophy of the oligotrophic oceans. Glob. Biogeochem. Cycles 26 (4), 106–113. http://dx.doi.org/10.1029/2011GB004094.

Williams, P.J.L., Quay, P.D., Westberry, T.K., Behrenfeld, M.J., 2013. The oligotrophic ocean is autotrophic. Annu. Rev. Mar. Sci. 5 5 (1), 535–549. http://dx.doi.org/10.1146/annurev-marine-121211-172335.

Wong, G.T.F., Tseng, C.M., Wen, L.S., Chung, S.W., 2007. Nutrient dynamics and N-anomaly at the SEATS station. Deep Sea Res. Part II: Top. Stud. Oceanogr. 54 (14), 1528–1545. http://dx.doi.org/10.4319/lo.2008.53.5_part_2.2226.

Wu, K., Dai, M., Chen, J., Meng, F., Li, X., Liu, Z., Du, C., Gan, J., 2015. Dissolved organic carbon in the South China Sea and its exchange with the Western Pacific Ocean. Deep Sea Res. Part II: Top. Stud. Oceanogr. 122, 41–51. http://dx.doi.org/10.1016/j.dsr2.2015.06.013.

Yang, B., Emerson, S.R., Bushinsky, S.M., 2017. Annual net community production in the subtropical Pacific Ocean from in-situ oxygen measurements on profiling floats. Glob. Biogeochem. Cycles. http://dx.doi.org/10.1002/2016GB005545.

Zhai, W.D., Dai, M.H., Chen, B.S., Guo, X.H., Li, Q., Shang, S.L., Zhang, C.Y., Cai, W.J., Wang, D.X., 2013. Seasonal variations of sea-air CO_2 fluxes in the largest tropical marginal sea (South China Sea) based on multiple-year underway measurements. Biogeosciences 10 (11), 7775–7791. http://dx.doi.org/10.5194/bg-10-7775-2013.

Zhang, W.Z., Wang, H.L., Chai, F., Qiu, G.Q., 2016. Physical drivers of chlorophyll variability in the open South China Sea. J. Geophys. Res.-Oceans 121 (9), 7123–7140. http://dx.doi.org/10.1002/2016jc011983.